Deposition and Aggregation Kinetics of Rotavirus in Divalent Cation Solutions

ARTICLE *in* ENVIRONMENTAL SCIENCE AND TECHNOLOGY · JUNE 2010

Impact Factor: 5.33 · DOI: 10.1021/es100120k · Source: PubMed

4 AUTHORS, INCLUDING:

Leonardo Gutierrez
Curtin University
19 PUBLICATIONS **215** CITATIONS
SEE PROFILE

Steven E. Mylon
Lafayette College
39 PUBLICATIONS **1,011** CITATIONS
SEE PROFILE

Thanh H Nguyen
University of Illinois, Urbana-Champaign
58 PUBLICATIONS **1,574** CITATIONS
SEE PROFILE

Environ. Sci. Technol. **2010,** *44,* 4552–4557

Deposition and Aggregation Kinetics of Rotavirus in Divalent Cation Solutions

LEONARDO GUTIERREZ,[†] STEVEN E. MYLON,[‡] BRIDGET NASH,[†] AND THANH H. NGUYEN*,[†]

Department of Civil and Environmental Engineering, the Center of Advanced Materials for the Purification of Water with Systems, University of Illinois at Urbana−Champaign, Urbana−Champaign, Illinois, and Department of Chemistry, Lafayette College, Easton, Pennsylvania

Received January 12, 2010. Revised manuscript received April 20, 2010. Accepted May 10, 2010.

Aggregation kinetics of rotavirus in aqueous solutions and its deposition kinetics on silica surface in the presence of divalent (Ca^{2+}, Mg^{2+}) cations were studied using complementary techniques of time-resolved dynamic light scattering (TR-DLS) and quartz crystal microbalance (QCM). Within a reasonable temporal window of 4 h, aggregation could be observed at levels as low as 10 mM of Ca^{2+} and 20 mM of Mg^{2+}. Attachment efficiencies were always greater in Ca^{2+} solutions of the same concentration, and the critical coagulation concentration (CCC) for rotavirus in Ca^{2+} solutions was slightly smaller than that in Mg^{2+} solutions. No aggregation was detected in Na^{+} solution within the temporal window of 4 h. Deposition experiments showed higher attachment coefficients in solutions containing Ca^{2+} compared to those obtained in Mg^{2+} solution. The classic Derjaguin−Landau−Verwey−Overbeek (DLVO) theory failed to predict both the aggregation behavior of rotavirus and its deposition on silica surface. Besides electrostatic interactions, steric repulsions and specific interactions with divalent cations were important mechanisms in controlling rotavirus deposition and aggregation. Experimental results presented here suggest that rotavirus is not expected to aggregate in groundwater with typical hardness (up to 6 mM Ca^{2+}) and rotavirus deposition on silica soil would be more favorable in the presence of Ca^{2+} than Mg^{2+}.

Introduction

Viruses are bionanoparticles responsible for a wide array of diseases in bacteria, plants, and animals, and cause a number of waterborne diseases (*1, 2*). While the number and diversity of viruses in soils, sediments, and freshwaters varies with host abundance and activity (*3*), they are routinely detected in private household wells, municipal wells, and even deep confined aquifers (*4*−*6*), and due, in part, to their small of size, viruses (20−80 nm) are generally more mobile than bacteria (0.5−3 μm) and protozoan parasites (4−15 μm) (*1*). In light of this, it is reasonable to conclude that viruses played a central role in the 76% of waterborne disease outbreaks in the United States that were linked to groundwater contamination (*7*) between 1991 and 2002.

Studies on virus fate and transport in natural aquatic systems have focused on the interaction of viruses at important environmental interfaces, specifically the mineral/water interface and the virus/virus interface. Results from examples of the former demonstrated the importance of electrostatic interactions in the specific situation of viral adsorption to solid interfaces. Using bacteriophages as surrogates for enteric viruses, the field data obtained in an aquifer containing iron oxide-coated sands suggested that electrostatic interactions control virus transport (*8*−*12*). In laboratory studies of the deposition of the bacteriophage MS2 onto both bare silica and organic matter coated silica, Yuan et al. (*13*) showed that increasing ionic strength resulted in increasing deposition rates due to the higher degree of charge screening. Virus/virus net attractive interactions were postulated by Langlet et al. (*14*) as they observed decreases in the mean apparent diffusion coefficient of virus suspensions with decreases in pH. As the pH approached the virus isoelectric point (IEP), or pH at which the virus carries no net electric charge, aggregation resulted from decreases in electrostatic repulsive interactions. Most recently, Mylon et al. (*15*) showed that MS2 exhibited extreme stability against aggregation in the presence of high concentrations of monovalent cations suggesting strong steric and electrosteric stabilization of MS2. In this study, however, divalent cations had a profound effect on the aggregation behavior of MS2 most likely because of complexation to charged moieties on the MS2 surface.

Groundwater contamination by enteric virus may cause serious public health concern (*4*), and therefore there is a need to study the interfacial interactions of these specific viruses. Some experimental evidence suggested that the use of MS2 and other well-studied bacteriophages as surrogates for enteric viruses may not be fully justified. For example, filtration experiments with bacteriophage MS2 and recombinant Norwalk virus particles suggest that bacteriophages may not be a suitable surrogate for virus transport experiments because of the different surface properties (*16*). Additionally, Gerba and Lance (*17*) observed that high concentrations of dissolved organic matter did not reduce attachment of polio virus where recent laboratory and field studies have demonstrated that under similar conditions bacteriophage attachment (*12, 18*) is reduced. The differences here most likely reflect the differences in surface properties between the bacteriophages MS2 and poliovirus.

Even though the use of MS2 as a model virus allows us to obtain a fundamental understanding of survivability and transport of viruses, there are important physical differences between bacteriophage MS2 and enteric viruses, including rotavirus, resulting in an obvious need for more studies using enteric viruses. For example, the protein capsid of MS2 is constructed from 180 single polypeptides. Each polypeptide consists of 129 amino acids (*19*). Intact rotavirus is a complex dsRNA triple-layered capsid (TLP) virus. Glycoprotein VP7 (calcium dependent trimer with a $T = 13$ icosahedral packing) and protein VP4 (60 monomers protruding as spikes) make up the outer capsid (*20, 21*). More important than the higher order structure differences between MS2 and rotavirus is the distribution of the charged amino acids glutamic acid, aspartic acid, and lysine about the outermost capsid. For rotavirus, there are 21 charged amino acids (6 aspartic acid, 9 glutamic acid, and 6 lysine) in one of the N-terminal proteins, VP8 (located on the tip of VP4). The specific chemistry of these charged moieties in aqueous solutions gives rise to the unique characteristics of each type of virus,

* Corresponding author e-mail: thn@illinois.edu.
[†] University of Illinois at Urbana−Champaign.
[‡] Lafayette College.

10.1021/es100120k

Published on Web 05/19/2010

such as pH-dependent surface potential and isoelectric point (i.e., pH_{IEP} of RV is ~4.5 whereas pH_{IEP} of MS2 is ~3.5) (*22*).

The objectives of this study are to probe the interfacial interactions of an enteric virus at the mineral/water interface using quartz crystal microbalance technique and the virus/virus interface using time-resolved dynamic light scattering, and to determine how important components of groundwater such as Ca^{2+} and Mg^{2+} might affect these interactions. Data interpretation is based on physical and chemical characteristics of viruses and theories developed for colloid and nanoparticle deposition and aggregation. For this study rotavirus has been selected because it is the most common enteric virus resulting in severe gastroenteritis among children worldwide (*23*).

Materials and Methods

Rotavirus Preparation and Infectivity Assays. Group A porcine rotavirus OSU strain (ATCC VR892) was propagated by MA-104 cells (African green monkey kidney cells) following the protocols described previously (*24*). Rotavirus was purified by centrifugation and micro- and nanofiltration (*22*). Focus forming assay (FFU) using MA-104 cells (*25*) was used for rotavirus enumeration. The final stock of rotavirus was stored at 4 °C at a final concentration of ~5×10^6 FFU/mL in 1 mM NaCl and 0.1 mM $CaCl_2$ which is required to prevent rotavirus dissolution due to structural changes in the outermost capsid of rotavirus. The critical free Ca^{2+} concentration that leads to the dissociation of the outermost capsid proteins (VP4 and VP7) of porcine OSU rotavirus was quantified as 100 nM (*26*).

Measurement of Electrophoretic Mobility (EPM) for Rotavirus. A Zetasizer ZS90 (Malvern, UK) and 1 mL clear disposable zeta cells (DTS1060C, Malvern, UK) were used for measuring the electrophoretic mobility of rotavirus. Rotavirus was added to desired electrolyte solutions (NaCl, $NaHCO_3$, $MgCl_2$, or $CaCl_2$) and DI water to a final concentration of ~8×10^5 FFU/mL. At least 3 measurements per sample were made. Zeta potentials was obtained by converting EPM using the Smoluchowski equation by Dispersion Technology Software (v5.10, 2008, Malvern, UK). The lowest concentrations of Ca^{2+} and Mg^{2+} employed in this study (0.1 mM to 10 mM) represents the hardness conditions found in natural groundwater in the United States (*27*). However aggregation rates for both divalent cations concentrations of 0.1 mM and 10 mM were still lower than the diffusion-limited aggregation rate. Therefore, for aggregation experiments we needed to employ even greater concentrations of Ca^{2+} to reach the critical coagulation concentration (CCC) (*15*).

Transmission Electron Microscopy (TEM). Micrographs of rotavirus were obtained by a cryo TEM (JEM-2100, JEOL, Tokyo, Japan) operating at 200 kV to ensure the integrity of rotavirus particles. Rotavirus pellets were obtained after centrifugation at 48 500*g* for 1 h. These pellets were recovered and resuspended using a few drops of Karnovsky's fixative for 20 min. The virus suspensions were applied to holey-carbon-coated copper grids of 300 mesh, and stained with uranyl acetate.

Measurement of Hydrodynamic Diameter of Rotavirus by Dynamic Light Scattering (DLS). Using a ZS90 Zetasizer (Malvern, UK) the initial hydrodynamic diameter of rotavirus was measured before every experiment which served as baseline measurements. This ZS90 Zetasizer utilizes a 4 mW HeNe laser operating at a wavelength of 633 nm. Low-volume plastic cuvettes (ZENO112, Malvern, UK) were used for each experiment and disposed after a single use. Scattered light intensity was measured by a photodiode positioned at a scattering angle of 90° from the incident laser beam. Autocorrelation functions were accumulated for 20 s and the corresponding intensity-weighted hydrodynamic diameter of the rotavirus particles was determined through second-order cumulant analysis by Dispersion Technology Software (v5.10, 2008, Malvern, UK). Rotavirus solutions were prepared by diluting stock suspensions with DI water until a final concentration of ~8×10^5 FFU/mL. This initial concentration ensured an attenuator setting on the ZS90 Zetasizer of 10 (i.e., 30% of maximum laser power transmitted). At least 3 measurements per solution condition were made.

Time-resolved dynamic light scattering was used to determine the aggregation kinetics of rotavirus in solutions of various concentration of either Na^+, Mg^{2+}, or Ca^{2+}. For each experiment, a rotavirus solution was prepared at the desired concentration of electrolyte solution. The solution was given a gentle shake and placed into the Zetasizer instrument as quickly as possible. Measurements began immediately and extended over 4 h to allow for an increase in the intensity-weighted hydrodynamic diameter by 38% of the initial hydrodynamic diameter (D_{ho}) (*28*).

Determination of Virus/Virus Attachment Efficiency (1/*W*). Rotavirus aggregation kinetics were determined by measuring the increase in hydrodynamic diameter (D_h) with time. The slope of the initial portion of this curve is directly proportional to the product of the aggregation rate constant (commonly, k_{11}) and the initial concentration of rotavirus (*28, 29*). From the initial slope, the attachment efficiency or inverse stability ratio, $1/W$, was calculated by normalizing the experimental aggregation rate constant, k_{11exp}, to the diffusion limited aggregation rate constant, $k_{11\ rapid}$ $1/W = k_{11exp}/k_{11rapid}$.

Determination of Deposition Kinetics by Quartz Crystal Microbalance (QCM). We employed a QCM-D D-300 instrument (Q-Sense, Gothenburg, Sweden) to monitor deposition kinetics experiments of rotavirus on silica and functionalized silica surfaces. A detailed method was reported in our earlier studies on the deposition of bacteriophage MS2 (*13, 30*). Briefly, QCM-D was used to determine the initial deposition rates of rotavirus in electrolyte solutions on silica surfaces in a radial stagnation flow point cell. As a proxy for naturally occurring silica surfaces, ultrasensitive silica sensors (Q-Sense, QSX 303 silica, batch 070117) coated with 50 nm amorphous silicon dioxide (SiO_2) were used. We confirmed that the oscillating frequency was proportional to the total adsorbed mass in separate experiments where the concentration of rotavirus in solution was doubled from 8×10^5 FFU/mL. We found that the deposition rate of rotavirus at the higher concentration of rotavirus was twice that of the lower concentration of rotavirus at the same concentration of background electrolyte (1 mM Ca^{2+}) confirming that the shift of frequency in time is directly proportional to the concentration of viruses adsorbed on the silica surface of the oscillating sensor. The frequency variations were monitored at 3 overtones ($n = 3, 5, 7$). For all the experiments, the initial shift of frequency as a function of time, or slope of the curve at the third overtone $f_{(3)}$, was calculated as rotavirus adsorption rate. For fair comparison, each rotavirus adsorption rate at a given electrolyte concentration condition was normalized by the rate of deposition onto PLL functionalized silica at the same electrolyte concentration (favorable deposition rate).

To ensure data quality and reproducibility of results, the quartz sensors were soaked for 2 h in a 2% Hellmanex II cleaning solution (Hellma GmbH & Co. KG, Mullheim, Germany). Afterward the sensor was rinsed with DI water, dried with ultrapure N_2, and exposed to ozone/UV for 30 min (BioForce Nanosciences, Inc., Ames, IA). The sensor was only used 5 times to ensure that experiments were performed with an intact silica surface (see SI for more information).

The flow rate for all experiments was 0.1 mL/min using a precision syringe pump (Kd Scientific Inc., Holliston, MA) operating in withdrawal mode. Prior to all experiments, the sensors were equilibrated with DI water for at least 30 min until a stable baseline (no more than 2 Hz change in frequency

over 1 h) was achieved. For deposition experiments on silica surface, 2 mL of our choice of electrolyte solution (NaCl, $MgCl_2$, or $CaCl_2$) at the concentration of interest was injected to the sensor chamber for equilibration. Following this step, deposition experiments were conducted by flowing 2 mL of rotavirus suspension at a concentration of $\sim 8 \times 10^5$ FFU/mL with the same electrolyte concentration as the previous step.

To create favorable deposition conditions the sensor was first functionalized with a PLL layer. After the equilibration period with DI water, 2 mL of HEPES buffer was injected to the sensor chamber. Once a stable baseline was achieved, the sensor was coated by flowing PLL in HEPES solution at a final concentration of 0.1 g/L. After functionalizing the sensor with PLL, 2 mL of HEPES buffer was flowed through the chamber and followed by 2 mL of the electrolyte solution at the concentration of interest.

DLVO Energy Profiles. The total interaction energy between rotavirus and the silica plate surface or between rotavirus particles was calculated as the sum of repulsive electrostatic and retarded van der Waals interactions (*31, 32*). Virus/virus interaction in aggregation experiments and virus/collector interaction in deposition experiments were calculated based on the DLVO energy profiles for sphere/sphere and sphere/plate, respectively. For the calculation, the zeta potential values were used as surface potential of the rotavirus and we used a mean value for proteins in water, 4×10^{-21} J, for the rotavirus Hamaker constant (A) (*33*).

Softness of Rotavirus and Ohshima Approximation. For nanoparticles consisting of heterogeneous polyelectrolyte macromolecules ("soft" charged particles) which describes functionalized hard particles, some bacterial cells, and other biological particles including some viruses, the calculated zeta potential can be a poor descriptor of the surface potential for the particle because the electrohydrodynamic interactions of soft charged particles are complicated by the unrelated anisotropies of both hydrodynamic permeability and charge density (*14, 34*). Therefore zeta potential, widely used for describing the electrokinetic behavior of "hard" particles, loses its meaning and instead the Donnan potential is used to determine the electrokinetics of "soft" particles. The theory developed by Ohshima (*35*) has been used to account for these differences. From this theory, two important parameters, electrophoretic softness and the outer surface potential, can be determined. Electrophoretic softness ($1/\lambda$) is defined as the thickness of the soft layer and outer surface potential is the potential at the boundary of the soft layer and the solution (*35*). When $1/\lambda$ approaches zero, the particle can be considered rigid. These parameters have been reported for bacteria, *Cryptosporidium* oocysts, and bacteriophage MS2 (*13, 15, 36, 37*). We calculated the electrophoretic softness of rotavirus by applying a curve-fitting procedure for the EPM data of rotavirus measured in Na^+ solution to the Ohshima equation.

Results and Discussion

Characterization of Rotavirus: Size, Electrophoretic Mobility (EPM), Surface Potential, and Softness. TEM micrographs of the rotavirus stock solution (Figure 1A) confirmed suspensions of intact viral particles with a mean diameter of 75 ± 1 nm (total rotavirus particles measured = 14) which is the same as previously reported (*22, 38*). No apparent structural damage of rotavirus protein capsid was observed as the VP4 proteins (commonly referred to as spikes) remained intact. The mean hydrodynamic diameter of rotavirus in aqueous solutions measured before each aggregation and deposition experiment was 113 ± 3 nm (Figure 1B). The mean polydispersivity index <0.25 of the cumulant analysis indicated that the rotavirus suspensions were monodisperse prior to each experiment. Differences between hydrodynamic and TEM diameters are well-known and result from the hydration

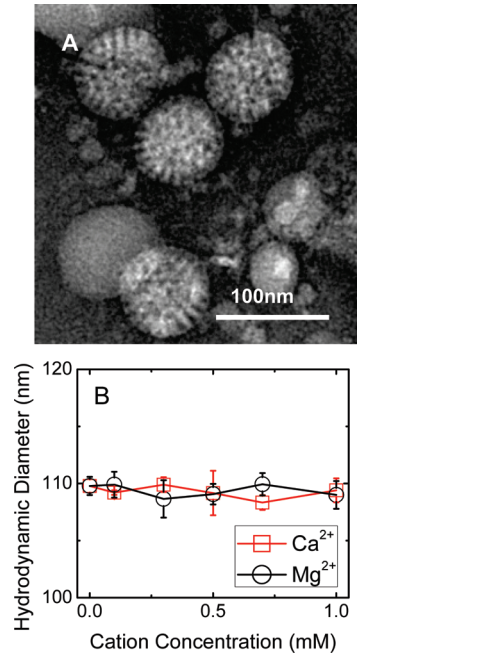

FIGURE 1. (A) TEM micrograph of rotavirus. Micrographs of rotavirus were obtained using a Cryo TEM at 200 kV accelerated voltage by conventional negative staining using uranyl acetate. The diameter of rotavirus based on TEM was ca. 75 nm. (B) Monodispersivity of rotavirus at low concentration of divalent cations. Hydrodynamic diameter of rotavirus at 25 °C and pH ~5.9 was measured at low concentrations of Mg^{2+} and Ca^{2+} (0 to 1 mM) prior to QCM experiments. The hydrodynamic diameter of virus particles in each suspension remained constant over the temporal window of our experiments (4 h).

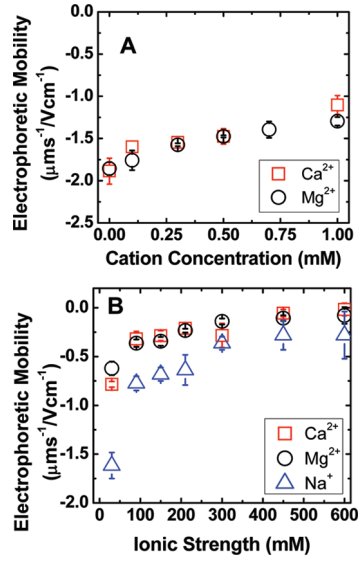

FIGURE 2. (A) Electrophoretic mobility of rotavirus in solutions of low concentrations of Ca^{2+} or Mg^{2+}. (B) Electrophoretic mobility of rotavirus in solutions with different background cations across a range of ionic strengths. All the EPM experiments were conducted at 25 °C and pH ~5.9 with an initial rotavirus concentration of $\sim 8 \times 10^5$ FFU/mL.

of rotavirus in solution during DLS measurements contrasted to the cryogenic process required for TEM imaging (*22, 39*).

With increasing cation concentration, the EPM of rotavirus became less negative (Figure 2A and B), and reached a limit close to 0 $\mu ms^{-1}/Vcm^{-1}$ at an ionic strength (IS) of 450 mM for divalent cations. The EPM of rotavirus in Na^+ solution

was always more negative than in divalent cation solution at the same IS (Table 2S, SI). Differences between the EPM of rotavirus in solutions of divalent vs monovalent cations are from the complexation of divalent cations with deprotonated carboxylic groups located on exposed polar charged amino acids (lysine, glutamic acid, or aspartic acid) present on the outermost capsids (glycoprotein VP7 and protein VP4) of rotavirus (*20, 21*), as previously observed in similar systems (*15*).

The electrophoretic mobility of rotavirus as a function of IS was used to calculate the outer surface potentials and electrophoretic softness using Ohshima's equation (*35*) for soft particles and zeta potentials using Smoluchowski's equation (*40*). Fits to Ohshima's equation were obtained for electrophoretic mobility data only at ionic strengths above 10 mM with the fixed charge density and electrophoretic softness used as fitting parameters. The electrophoretic softness, $1/\lambda$, is described in terms of length units where $\lambda = \sqrt{(\gamma/\eta)}$ and η is the viscosity and γ is the frictional coefficient of the soft layer (*35*). For rotavirus, the $1/\lambda = 0.5$ nm. As a first approximation the difference in electrophoretic softness of rotavirus compared to that of MS2 ($1/\lambda = 2.3$ nm) (*15*) indicates that rotavirus behaves more like a hard sphere than MS2 and therefore DLVO theory is an appropriate choice for modeling its aggregation and deposition behavior. For comparison, in a recent study for silica particles ($R_H \sim 1.6$ μm in diameter) which are commonly used as model hard spheres, $1/\lambda$ was calculated to be 0.32 nm (*36*).

Aggregation Kinetics of Rotavirus in Monovalent or Divalent Cation Solutions. Rotavirus stability was investigated under a wide range of solution conditions. We employed Na^+, Ca^{2+}, or Mg^{2+} cations as supporting electrolytes at pH = 5.9. In Na^+ solution across an IS from 30 mM to 600 mM, rotavirus remained stable against aggregation over the 4 h experimental window. The same trend was observed in our previous research using the bacteriophage MS2 (*15*).

Like MS2, the stability of rotavirus is inconsistent with the predictions of DLVO theory for sphere/sphere interactions. Based on experimental surface potentials for rotavirus, diffusion-limited aggregation should be observed at $[Na^+] >$ 90 mM (Table 1S, SI). Our results suggest non-DLVO forces are primarily responsible for these stable suspensions of rotavirus. We posit that the VP4 proteins on the capsid contribute steric repulsive forces that prevent the aggregation of rotavirus even at very large Na^+ concentrations. Steric interactions in microorganisms have been extensively studied (*41*−*43*). In these systems the long-range repulsive forces are primarily steric in nature consistent with polyelectrolyte brush layer in microorganisms surfaces. Similar protein loops on the MS2 surface may be responsible for its stability as well (*30, 33*). Steric and electrosteric interactions have been invoked to explain the significant decrease in the aggregation rates of polystyrene latex, organic matter coated hematite, and C_{60} in the presence of monovalent cations Na^+ and K^+ (*28, 29, 44*), but in these systems aggregation has never been eliminated as it is in the case of rotavirus and MS2 in the monovalent electrolytes.

In contrast to its stability in the presence of Na^+, rotavirus aggregates in both Mg^{2+} and Ca^{2+} solutions (Figure 3A). The aggregation rate of rotavirus increased as the Mg^{2+} concentration was increased from 20 to 100 mM indicating reaction limited or unfavorable aggregation of rotavirus. At Mg^{2+} concentrations above ca.120 mM, the aggregation rate remained constant which is indicative of favorable aggregation. Defined by the crossover region between favorable and unfavorable aggregation regimes, the critical coagulation concentration (CCC) for rotavirus in Mg^{2+} is 120 mM. In Ca^{2+} solution, aggregation of rotavirus could also be induced although the CCC is slightly lower compared to the case of

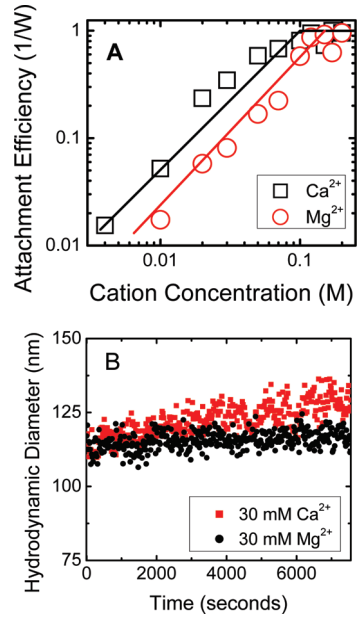

FIGURE 3. (A) Attachment efficiency (1/*W*) of rotavirus in the presence of divalent cations. Aggregation rates for rotavirus were measured at various cation concentrations ranging from 4 mM to 200 mM in Ca^{2+} and 10 mM to 200 mM in Mg^{2+} and normalized as attachment efficiency with respect to the fastest measured aggregation rate (the lines are meant to delineate the regions between favorable and unfavorable aggregation). (B) Change of hydrodynamic diameter of rotavirus with time in the presence of divalent cations. Aggregation rate of rotavirus was measured in the presence of 30 mM Ca^{2+} and 30 mM Mg^{2+}. Measurements were recorded every 20 s. These TR-DLS experiments were conducted at 25 °C and pH ~5.9.

Mg^{2+}. The results shown in Figure 3 are the calculated stability ratios ($1/W$) obtained for rotavirus in both Ca^{2+} and Mg^{2+} solutions.

The results of molecular dynamic simulation suggest that cation−NOM binding takes place predominantly with carboxylate groups and the strength of the cation−carboxylate complexation can be described using the ratio of charge/radius of the cation involved. Although Ca^{2+} and Mg^{2+} have the same charge, Ca^{2+} is expected to interact more strongly than Mg^{2+} because of a larger ionic radius ($R_{Ca^{2+}} = 1.61$ Å, $R_{Mg^{2+}} = 0.92$ Å) (*45, 46*). As a smaller cation, Mg^{2+} has a strongly held hydration sphere and thus only weak outer sphere complexes to the organic moiety can be expected. The larger Ca^{2+} cation can exchange water more easily forming inner sphere complexes with carboxylate groups. Glycoprotein VP7 and protein VP4 on the outermost capsids of rotavirus are known to contain the amino acids glutamic acid or aspartic acid, both of which contain carboxylate moieties (*20, 21*). Thus, inner sphere and outer sphere complexation of Ca^{2+} and Mg^{2+}, respectively, with carboxylate groups on rotavirus surface leads to higher rates of aggregation in Ca^{2+} compared to Mg^{2+} solution.

We also employed DLVO theory to predict the energy barrier to aggregation for the system of rotavirus in both Ca^{2+} and Mg^{2+} solutions. Based on these calculations no energy barrier to aggregation was predicted, and diffusion limited aggregation, $1/W = 1$ was expected at all the experimental concentrations. The theory of DLVO, however, does not consider steric or electrosteric interactions (*40*), and the enhanced stability cannot be predicted within the DLVO paradigm. This discrepancy between the stability of rotavirus suspensions where the supporting electrolyte is monovalent compared to those suspensions in divalent cations is most likely due to the formation of complexes between divalent cations and functional groups on rotavirus

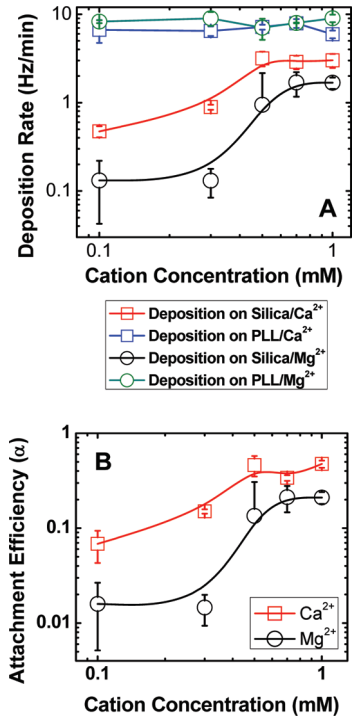

FIGURE 4. (A) Deposition kinetics of rotavirus on silica surface and PLL-coated silica surface in the presence of divalent cations. The cation concentration (Ca^{2+} and Mg^{2+}) ranged from 0.1 to 1 mM for all the experiments. The temperature of the experiments was 25 °C at an initial rotavirus concentration of 8 × 10^5 FFU/mL and a pH of 5.9. The deposition rates were expressed in Hz/min (all lines are drawn as guides). (B) Attachment efficiencies of rotavirus on silica surface. Deposition rates of rotavirus on silica surface were normalized by the deposition rate on PLL surface for each cation condition (Ca^{2+} and Mg^{2+}).

outermost capsid. Complexation of divalent cations to the charged functional groups of the rotavirus capsid probably alters the structure of key components to the protein capsid which must have a diminishing effect on the steric forces that are responsible the stability of rotavirus. Enhanced aggregation of nanoparticles due to specific interactions between divalent cations and organic matter has been previously studied (*47, 48*), and divalent cations (Ba^{2+}, Ca^{2+}, Sr^{2+}) were hypothesized to complex with charged functional groups from materials (NOM, alginate) that were adsorbed to the surface of the colloids. In some cases, this has resulted in substantial increase aggregation rates compared to the same solutions in monovalent electrolytes (*47, 48*).

Rotavirus Deposition Kinetics to Silica Surface. Prior to all deposition experiments the monodispersity of rotavirus suspensions in Ca^{2+} and Mg^{2+} (0.1 to 1 mM) solution were measured using DLS. As shown in Figure 1B, the suspensions were stable against aggregation and remained so for at least 30 min.

We defined favorable deposition as the rotavirus/PLL system because at the pH 5.9 rotavirus is negatively charged (*22*) while PLL is positively charged. Deposition rates of rotavirus under favorable conditions to PLL-coated silica surface in the presence of Ca^{2+} remained reasonably stable over the range of concentrations employed (Figure 4A). Deposition kinetics of rotavirus to the bare silica surface (repulsive conditions) in the presence of Ca^{2+} is shown in Figure 4A. At a concentration of 0.1 mM Ca^{2+} the deposition rate was approximately 14 times lower than favorable conditions at the same Ca^{2+} concentration. We observed an increase in the adsorption rate of rotavirus with concomitant increase in Ca^{2+} concentration. At 0.3 mM Ca^{2+}, the deposition rate increased to 7 times lower than those on PLL surface, and an apparent maximum deposition rate was reached by 0.5 mM Ca^{2+}. The fact that the maximum deposition rate was still lower (2.3 times) than that measured under favorable attachment conditions has been observed in previous studies where attachment efficiencies measured under experimental conditions never reach unity. For example, the maximum attachment efficiency of 0.7 was measured for bacteriophage MS2 deposition on silica surface coated with Suwannee River Natural Organic Matter (*30*) and bacteriophage lambda on sand collector (*33*).

Although DLVO theory predicts similar energy barrier for adsorption of rotavirus to bare silica in Ca^{2+} and Mg^{2+} solutions of the same concentration (Table 1S, SI), our experimental attachment efficiencies for rotavirus adsorption to silica surface in Mg^{2+} solution were always lower than the corresponding solution in Ca^{2+} solution (Figure 4B). This contrasts some earlier studies where the adsorption rate in Ca^{2+} compared to Mg^{2+} was greater for plasmid DNA and bacteriophage MS2 adsorption (*30, 49*). The differences in the solution chemistry and complexation characteristics between Mg^{2+} and Ca^{2+} that were discussed previously are most likely responsible for these differences between rotavirus attachment efficiencies.

Environmental Implications of Rotavirus Deposition and Aggregation Kinetics. This and other studies show that van der Waals and electrostatic interactions alone do not govern the interactions of viruses at interfaces (virus/virus or virus/solid) (*13, 15, 30*). Rotavirus aggregation was not measurable under the solution conditions that typify groundwater hardness in the United States (up to 6 mM Ca^{2+} and Mg^{2+}) (*27*). Even at much higher levels of hardness the rotavirus concentrations in contaminated groundwater do not reach the concentrations that we employed in these aggregation experiments. Therefore, the aggregation of rotavirus is unlikely the common fate in natural aquatic systems. Deposition of rotavirus on silica surface, however, was significant at these concentrations, and therefore, the interactions of rotavirus at the mineral/water interface are more likely to govern their fate and transport in the subsurface media. The stability of viruses against aggregation and to some extent deposition reported in this study together with other field studies (*4*−*6, 27*) suggests that viruses (infectious and noninfectious) are uniquely mobile in aquatic systems.

Acknowledgments

This work was partially supported by the WaterCAMPWS NSF grant CTS-0120978, USDA grant 2008-35102-19143, NSF CAREER award to T.H.N. (0954501), and NSF-MRI Grant 0619409.

Supporting Information Available

This material is available free of charge via the Internet at http://pubs.acs.org.

Literature Cited

(1) Abbaszadegan, M.; Lechevallier, M.; Gerba, C. Occurrence of viruses in US groundwaters. *J. Am. Water Works Assoc.* **2003**, *95* (9), 107–120.

(2) Yoder, J. S.; Hlavsa, M. C.; Craun, G. F.; Hill, V.; Roberts, V.; Yu, P. A.; Hicks, L. A.; Alexander, N. T.; Calderon, R. L.; Roy, S. L.; Beach, M. J. *Surveillance for Waterborne Disease and Outbreaks Associated with Recreational Water Use and Other Aquatic Facility-Associated Health Events - United States, 2005*−*2006*; CDC: 2008.

(3) Masen, E. L. *Environmental Microbiology: From Genomes to Biogeochemistry*; Wiley-Blackwell, 2008.

(4) Borchardt, M. A.; Bertz, P. D.; Spencer, S. K.; Battigelli, D. A. Incidence of enteric viruses in groundwater from household wells in Wisconsin. *Appl. Environ. Microbiol.* **2003**, *69* (2), 1172–1180.

(5) Borchardt, M. A.; Haas, N. L.; Hunt, R. J. Vulnerability of drinking-water wells in La Crosse, Wisconsin, to enteric-virus contamination from surface water contributions. *Appl. Environ. Microbiol.* **2004**, *70* (10), 5937–5946.
(6) Borchardt, M. A.; Bradbury, K. R.; Gotkowitz, M. B.; Cherry, J. A.; Parker, B. L. Human enteric viruses in groundwater from a confined bedrock aquifer. *Environ. Sci. Technol.* **2007**, *41* (18), 6606–6612.
(7) Hoffman, R.; Marshall, M. M.; Gibson, M. C.; Rochelle, P. A. Prioritizing Pathogens for Potential Future Regulation in Drinking Water. *Environ. Sci. Technol.* **2009**, *43* (14), 5165–5170.
(8) Abudalo, R. A.; Bogatsu, Y. G.; Ryan, J. N.; Harvey, R. W.; Metge, D. W.; Elimelech, M. Effect of ferric oxyhydroxide grain coatings on the transport of bacteriophage PRD1 and *Cryptosporidium parvum* oocysts in saturated porous media. *Environ. Sci. Technol.* **2005**, *39* (17), 6412–6419.
(9) Harvey, R. W.; Ryan, J. N. Use of PRDI bacteriophage in groundwater viral transport, inactivation, and attachment studies. *FEMS Microbiol. Ecol.* **2004**, *49* (1), 3–16.
(10) Ryan, J. N.; Harvey, R. W.; Metge, D.; Elimelech, M.; Navigato, T.; Pieper, A. P. Field and laboratory investigations of inactivation of viruses (PRD1 and MS2) attached to iron oxide-coated qauartz sand. *Environ. Sci. Technol.* **2002**, *36* (11), 2403–2413.
(11) Ryan, J. N.; Elimelech, M.; Ard, R. A.; Harvey, R. W.; Johnson, P. R. Bacteriophage PRD1 and silica colloid transport and recovery in an iron oxide-coated sand aquifer. *Environ. Sci. Technol.* **1999**, *33* (1), 63–73.
(12) Pieper, A. P.; Ryan, J. N.; Harvey, R. W.; Amy, G. L.; Illangasekare, T. H.; Metge, D. W. Transport and recovery of bacteriophage PRD1 in a sand and gravel aquifer: Effect of sewage-derived organic matter. *Environ. Sci. Technol.* **1997**, *31* (4), 1163–1170.
(13) Yuan, B. L.; Pham, M.; Nguyen, T. H. Deposition Kinetics of Bacteriophage MS2 on a Silica Surface Coated with Natural Organic Matter in a Radial Stagnation Point Flow Cell. *Environ. Sci. Technol.* **2008**, *42* (20), 7628–7633.
(14) Langlet, J.; Gaboriaud, F.; Gantzer, C.; Duval, J. F. L. Impact of chemical and structural anisotropy on the electrophoretic mobility of spherical soft multilayer particles: The case of bacteriophage MS2. *Biophys. J.* **2008**, *94* (8), 3293–3312.
(15) Mylon, S. E.; Rinciog, C. I.; Schmidt, N.; Gutierrez, L.; Wong, G. C. L.; Nguyen, T. H. Influence of Salts and Natural Organic Matter on the Stability of Bacteriophage MS2. *Langmuir* **2010**, *26* (2), 1035–1042.
(16) Redman, J. A.; Grant, S. B.; Olson, T. M.; Hardy, M. E.; Estes, M. K. Filtration of recombinant Norwalk virus particles and bacteriophage MS2 in quartz sand: Importance of electrostatic interactions. *Environ. Sci. Technol.* **1997**, *31* (12), 3378–3383.
(17) Gerba, C. P.; Lance, J. C. Poliovirus Removal from Primary and Secondary Sewage Effluent by Soil Filtration. *Appl. Environ. Microbiol.* **1978**, *36* (2), 247–251.
(18) Zhuang, J.; Jin, Y. Virus retention and transport as influenced by different forms of soil organic matter. *J. Environ. Qual.* **2003**, *32* (3), 816–823.
(19) Golmohammadi, R.; Valegard, K.; Fridborg, K.; Liljas, L. The Refined Structure of Bacteriophage-Ms2 at 2-Center-Dot-8-Angstrom Resolution. *J. Mol. Biol.* **1993**, *234* (3), 620–639.
(20) Aoki, S. T.; Settembre, E. C.; Trask, S. D.; Greenberg, H. B.; Harrison, S. C.; Dormitzer, P. R. Structure of Rotavirus Outer-Layer Protein VP7 Bound with a Neutralizing Fab. *Science* **2009**, *324* (5933), 1444–1447.
(21) Dormitzer, P. R.; Sun, Z. Y. J.; Wagner, G.; Harrison, S. C. The rhesus rotavirus VP4 sialic acid binding domain has a galectin fold with a novel carbohydrate binding site. *EMBO J.* **2002**, *21* (5), 885–897.
(22) Gutierrez, L.; Li, X.; Wang, J.; Nangmenyi, G.; Economy, J.; Kuhlenschmidt, T. B.; Kuhlenschmidt, M. S.; Nguyen, T. H. Adsorption of rotavirus and bacteriophage MS2 using glass fiber coated with hematite nanoparticles. *Water Res.* **2009**, *43* (20), 5198–5208.
(23) Parashar, U. D.; Gibson, C. J.; Bresee, J. S.; Glass, R. I. Rotavirus and severe childhood diarrhea. *Emerg. Infect. Dis.* **2006**, *12* (2), 304–306.
(24) Rolsma, M. D.; Gelberg, H. B.; Kuhlenschmidt, M. S. Assay for Evaluation of Rotavirus-Cell Interactions - Identification of an Enterocyte Ganglioside Fraction That Mediates Group-a Porcine Rotavirus Recognition. *J. Virol.* **1994**, *68* (1), 258–268.
(25) Rolsma, M. D.; Kuhlenschmidt, T. B.; Gelberg, H. B.; Kuhlenschmidt, M. S. Structure and function of a ganglioside receptor for porcine rotavirus. *J. Virol.* **1998**, *72* (11), 9079–9091.
(26) Ruiz, M. C.; Charpilienne, A.; Liprandi, F.; Gajardo, R.; Michelangeli, F.; Cohen, J. The concentration of Ca2+ that solubilizes outer capsid proteins from rotavirus particles is dependent on the strain. *J. Virol.* **1996**, *70* (8), 4877–4883.
(27) Yates, M. V.; Gerba, C. P.; Kelley, L. M. Virus Persistence in Groundwater. *Appl. Environ. Microbiol.* **1985**, *49* (4), 778–781.
(28) Holthoff, H.; Egelhaaf, S. U.; Borkovec, M.; Schurtenberger, P.; Sticher, H. Coagulation rate measurements of colloidal particles by simultaneous static and dynamic light scattering. *Langmuir* **1996**, *12* (23), 5541–5549.
(29) Chen, K. L.; Mylon, S. E.; Elimelech, M. Aggregation kinetics of alginate-coated hematite nanoparticles in monovalent and divalent electrolytes. *Environ. Sci. Technol.* **2006**, *40* (5), 1516–1523.
(30) Pham, M.; Nguyen, T. H. Deposition Kinetics of Bacteriophage MS2 to Natural Organic Matter: Role of Divalent Cations. *J. Colloid Interface Sci.* **2009**, *338* (1), 1–9.
(31) Gregory, J. Approximate Expressions for Retarded Van der Waals Interaction. *J. Colloid Interface Sci.* **1981**, *83* (1), 138–145.
(32) Hogg, R.; Healy, T. W.; Fuersten, Dw. Mutual Coagulation of Colloidal Dispersions. *Trans. Faraday Soc.* **1966**, *62* (522P), 1638.
(33) Penrod, S. L.; Olson, T. M.; Grant, S. B. Deposition kinetics of two viruses in packed beds of quartz granular media. *Langmuir* **1996**, *12* (23), 5576–5587.
(34) Langlet, J.; Gaboriaud, F.; Duval, J. F. L.; Gantzer, C. Aggregation and surface properties of F-specific RNA phages: Implication for membrane filtration processes. *Water Res.* **2008**, *42* (10−11), 2769–2777.
(35) Ohshima, H. Electrokinetics of soft particles. *Colloid Polym. Sci.* **2007**, *285* (13), 1411–1421.
(36) de Kerchove, A. J.; Elimelech, M. Relevance of electrokinetic theory for "soft" particles to bacterial cells: Implications for bacterial adhesion. *Langmuir* **2005**, *21* (14), 6462–6472.
(37) Liu, Y. Y.; Janjaroen, D.; Kuhlenschmidt, M. S.; Kuhlenschmidt, T. B.; Nguyen, T. H. Deposition of *Cryptosporidium parvum* Oocysts on Natural Organic Matter Surfaces: Microscopic Evidence for Secondary Minimum Deposition in a Radial Stagnation Point Flow Cell. *Langmuir* **2009**, *25* (3), 1594–1605.
(38) Estes, M. K.; Cohen, J. Rotavirus Gene Structure and Function. *Microbiol. Rev.* **1989**, *53* (4), 410–449.
(39) Lute, S.; Aranha, H.; Tremblay, D.; Liang, D. H.; Ackermann, H. W.; Chu, B.; Moineau, S.; Brorson, K. Characterization of coliphage PR772 and evaluation of its use for virus filter performance testing. *Appl. Environ. Microbiol.* **2004**, *70* (8), 4864–4871.
(40) Elimelech, M.; Gregory, J.; Jia, X.; Williams, R. A. *Particle Deposition and Aggregation: Measurement, Modeling, and Simulation*; Butterworth-Heinemann: Oxford, 1995.
(41) Kuznar, Z. A.; Elimelech, M. Adhesion kinetics of viable *Cryptosporidium parvum* oocysts to quartz surfaces. *Environ. Sci. Technol.* **2004**, *38* (24), 6839–6845.
(42) Kuznar, Z. A.; Elimelech, M. Role of surface proteins in the deposition kinetics of *Cryptosporidium parvum* oocysts. *Langmuir* **2005**, *21* (2), 710–716.
(43) Byrd, T. L.; Walz, J. Y. Investigation of the interaction force between *Cryptosporidium parvum* oocysts and solid surfaces. *Langmuir* **2007**, *23* (14), 7475–7483.
(44) Chen, K. L.; Elimelech, M. Relating Colloidal Stability of Fullerene (C-60) Nanoparticles to Nanoparticle Charge and Electrokinetic Properties. *Environ. Sci. Technol.* **2009**, *43* (19), 7270–7276.
(45) Kalinichev, A. G.; Kirkpatrick, R. J. Molecular dynamics simulation of cationic complexation with natural organic matter. *Eur. J. Soil Sci.* **2007**, *58* (4), 909–917.
(46) Xu, X.; Kalinichev, A. G.; Kirkpatrick, R. J. 133Cs and Cl-35 NMR spectroscopy and molecular dynamics modeling of Cs+ and Cl−complexation with natural organic matter. *Geochim. Cosmochim. Acta* **2006**, *70* (17), 4319–4331.
(47) Mylon, S. E.; Chen, K. L.; Elimelech, M. Influence of natural organic matter and ionic composition on the kinetics and structure of hematite colloid aggregation: Implications to iron depletion in estuaries. *Langmuir* **2004**, *20* (21), 9000–9006.
(48) Chen, K. L.; Mylon, S. E.; Elimelech, M. Enhanced aggregation of alginate-coated iron oxide (hematite) nanoparticles in the presence of calcium, strontium, and barium cations. *Langmuir* **2007**, *23* (11), 5920–5928.
(49) Nguyen, T. H.; Chen, K. L. Role of divalent cations in plasmid DNA adsorption to natural organic matter-coated silica surface. *Environ. Sci. Technol.* **2007**, *41* (15), 5370–5375.

ES100120K